# Title: Perforin-2 is a pore-forming effector of endocytic escape in cross-presenting dendritic cells

**Authors:** Pablo Rodríguez-Silvestre[1], Marco Laub[1], Alexandra K. Davies[2], Julia P. Schessner[2], Patrycja A. Krawczyk[1], Benjamin J. Tuck[1,3], William A. McEwan[3], Georg H.H. Borner[2], Patrycja Kozik[1,*]

**Affiliations:**

[1] MRC Laboratory of Molecular Biology; Cambridge, UK.

[2] Department of Proteomics and Signal Transduction, Max Planck Institute of Biochemistry; Martinsried, Germany.

[3] UK Dementia Research Institute at the University of Cambridge, Department of Clinical Neurosciences; Cambridge, UK.

*** Corresponding author:**
Patrycja Kozik
E-mail:pkozik@mrc-lmb.cam.ac.uk

## Abstract:

During initiation of antiviral and antitumour T cell-mediated immune responses, dendritic cells (DCs) cross-present exogenous antigens on MHC class I. Cross-presentation relies on the unique 'leakiness' of endocytic compartments in DCs, whereby internalised proteins escape into the cytosol for proteasome-mediated generation of MHC I-binding peptides. Given that type 1 conventional DCs excel at cross-presentation, we searched for cell-type specific effectors of endocytic escape. We devised an escape assay suitable for genetic screening and identified a pore-forming protein, perforin-2, as a dedicated effector exclusive to cross-presenting cells. Perforin-2 is recruited to antigen-containing compartments, where it undergoes maturation, releasing its pore-forming domain. *Mpeg1*$^{-/-}$ mice fail to efficiently prime CD8$^{+}$ T cells to cell-associated antigens, revealing an important role of perforin-2 in cytosolic entry of antigens during cross-presentation.

## One-Sentence Summary:

Pore-forming protein perforin-2 is a dedicated effector of endocytic escape specific to cross-presenting cells

## Main text

The integrity of endosomal and lysosomal membranes is critical to protect the cell against extracellular pathogens and toxins, as well as from the activity of lysosomal hydrolases. Yet dendritic cells (DCs) allow internalised proteins to be delivered from endocytic organelles into the cytosol where they can be proteolytically processed for presentation on MHC class I molecules (*1*). The ability of dendritic cells to present exogenous peptides on endogenous MHC class I is termed cross-presentation and is critical for initiation of cytotoxic T cell (CTL) immune responses to antigens not expressed in DCs such as tumour neoantigens or antigens derived from virally infected cells (*2–4*).

Cross-presentation via the endosome-to-cytosol pathway was first reported over 20 years ago (*5*). Since then, various mechanisms have been shown to facilitate endocytic escape and promote cross-presentation (*6–10*). Early studies proposed that escape is mediated by protein channels (such as Sec61), which are recruited from the endoplasmic reticulum to endosomes in cross-presenting cells (*7*). More recent data suggest that escape occurs through unrepaired damage to endosomal membranes (e.g., due to ROS-driven lipid peroxidation) (*6*, *9*, *10*). Both models imply that the unusual 'leakiness' of endocytic compartments in cross-presenting DCs might not rely on any cell type-specific effectors, but rather on the regulation of ubiquitously expressed proteins through signalling (*11*, *12*) and trafficking (*13*) events unique to cross-presenting cells.

To gain a better understanding of how cross-presenting cells control endocytic escape, we set out to perform a genetic screen for DC-specific regulators. To this end, we developed a flow cytometry-based strategy to monitor endocytic escape in individual cells and adopted it for a CRISPR/Cas9-based screen in a cell type specialised in cross-presentation, conventional dendritic cells 1 (cDC1).

### Saporin-puromycin assay to monitor the efficiency of antigen import

To monitor endocytic escape in cross-presenting DCs, we used a type I ribosome inactivating protein (RIP) saporin (Fig. 1A) (*5*). Once in the cytosol, RIPs cause rapid translation arrest through depurination of the sarcin-ricin loop in the 28 subunit of the ribosome (*14*). While type II RIPs, such as ricin, comprise a domain that facilities entry into the cytosol, cytosolic delivery of type I RIPs is dependent on the cell intrinsic efficiency of endosome-to-cytosol transport (*5*). To detect saporin-induced translation inhibition, we used puromycin, a structural analogue of aminoacyl tRNAs, which is incorporated into nascent polypeptides at a rate that correlates with translation efficiency (*15–17*). Intracellular puromycylated polypeptides can be labelled with a fluorescent monoclonal antibody to puromycin (12D10) allowing for flow cytometry-based readout of translation efficiency and thereby of endocytic escape (Fig. 1A).

cDC1s, a subset of DCs that excels in cross-presentation *in vivo*(*18*) have been reported to have the most efficient endocytic escape pathway (*18*, *19*). Therefore, we set up the assay using a murinecDC1-like cell line, MutuDCs (*12*, *20*, *21*). A 30 min pulse with puromycin led to its efficient incorporation which could be blocked by a 2 h pretreatment with the translation

inhibitor cycloheximide confirming that puromycylation in MutuDCs is sensitive to changes in the rate of translation (fig. S1A). Next, we pulsed the cells with saporin and observed an increase in the number of cells with low puromycin signal indicating translation arrest due to saporin escape (Fig. 1B). The saporin-induced translational arrest was dose-dependent (Fig. 1C), confirming that our assay can accurately measure the efficiency of endocytic escape.

To demonstrate that endocytic escape of saporin is the rate-limiting step in the saporin-puromycin assay, we disrupted the integrity of endocytic compartments with glycyl-L-phenylalanine 2-naphthylamide (GPN). GPN is a cathepsin C substrate that induces osmotic lysis of lysosomes leading to release of lysosomal contents (*22*). In MutuDCs, 33 µM GPN caused endocytic damage visualised by staining for galectin 3, a marker of damaged compartments (*23*) (Fig. 1D). In the saporin-puromycin assay, the population of cells with arrested translation appeared with faster kinetics in the presence of GPN, confirming endocytic escape of saporin is rate-limiting in the saporin-puromycin assay (Fig. 1E).

**The saporin-puromycin assay recapitulates physiologically relevant differences in the efficiency of endocytic escape**

To test whether the saporin-puromycin assay can capture physiological differences in the efficiency of endocytic escape, we first focused on primary murine DCs subsets, cDC1s and cDC2s (previously reported as less efficient in antigen import and cross-presentation than cDC1s (*19*)). We performed the saporin-puromycin assay *ex vivo,* on splenic cDCs isolated by negative selection, and, in agreement with previous data, we demonstrated that saporin escape was more efficient in cDC1s (Fig. 1F).

We also analysed the efficiency of saporin escape in DCs from lupus-prone mice, homozygous for the lymphoproliferation spontaneous mutation (MRL/MpJ-Fas$^{lpr}$/J). Macrophages from the MRL mice have a defect in lysosomal stability resulting in leakage of lysosomal contents and excessive activation of cytosolic sensors (*24*). We performed the saporin-puromycin assay on CD11c$^{+}$ pre-enriched splenic DCs and found that saporin entered the cytosol more efficiently in cDC1s (and cDC2s) from the MRL mice compared to wild type C57BL/6J (Fig. 1G). Together, these experiments demonstrate that the saporin-puromycin assay recapitulates previously observed differences in the efficiency of endocytic escape.

**A CRISPR/Cas9 screen for regulators of endocytic escape**

To identify regulators of endocytic escape in DCs, we employed the saporin-puromycin assay in a CRISPR/Cas9 genetic screen. Considering the difference in efficiency of endocytic escape between the cDC1 and cDC2s (*25*) (Fig. 1F), we focused on 281 genes highly expressed in cDC1s (Fig. 2A). We generated a lentiviral mini-library using a BFP-containing plasmid, where each of the upregulated genes was targeted with four sgRNAs (Fig. 2B). We infected $4x10^6$ MutuDCs stably expressing Cas9, sorted for BFP$^{+}$ cells four days later, and expanded the cell library for a minimum of 10 days. We confirmed that all sgRNAs were recovered from MutuDCs when compared to the original plasmid library (table S1), except for sgRNAs targeting *Irf8*, which were significantly depleted (Fig. 2C). Considering Irf8 is a transcription factor required for cDC1

differentiation and for survival of terminally differentiated cDC1s (*26*), this analysis confirmed the suitability of MutuDCs as a cDC1 model system and demonstrated that the efficiency of gene editing in MutuDCs is sufficient for genetic screening.

To identify genes required for endocytic escape, we performed the saporin-puromycin assay using 0.5 mg/mL saporin spiked 11:1 with fluorescently labelled saporin-Atto 550. To ensure that the difference in puromycin incorporation was not due to a difference in uptake efficiency, we only collected the cells that took up similar amounts of saporin (Fig. 2C). We sorted the cells into two bins: puro$^{low}$ (saporin escape and translation arrest) and puro$^{high}$ (saporin retention and efficient translation). To control for possible differences in puromycin incorporation due to saporin-independent inhibition of translation, we also collected puro$^{low}$ and puro$^{high}$ populations from MutuDCs labelled in the absence of saporin. None of the sgRNAs affected the overall translation rate (Fig. 2D). The strongest hit identified in saporin-pulsed cells was *Mpeg1*, with four *Mpeg1*-targetting sgRNAs enriched in puro$^{low}$ vs puro$^{high}$ populations (Fig. 2E and fig. S2A).

**Perforin-2 is necessary for endocytic escape in DCs**

*Mpeg1* encodes perforin-2, a member of the membrane attack complex (MAC) and perforin superfamily (MACPF) of pore-forming proteins (*27*). Recent cryo-EM studies demonstrated that, like perforin-1 and complement, perforin-2 can form oligomeric pores on liposomes (*28*, *29*) (Fig. 3A). It has been initially proposed that the function of the perforin-2 pores is to facilitate killing of intravacuolar bacteria in infected cells (*30*), but these results were not replicated in a more recent study (*31*). Here, we explored whether perforin-2 can function as an effector of endocytic escape in DCs. To this end, we generated a *Mpeg1*$^{KO}$ MutuDC line by combining two sgRNAs targeting *Mpeg1* (expressed from a BFP-containing plasmid) and confirmed protein depletion in sorted BFP$^{+}$ cells by Western Blotting (fig. S2B). To account for the effect of passage numbers on MutuDCs behaviour (*21*), we cultured control cells expressing non-targeting (NT) sgRNA in parallel with the KO line.

Since translation inhibition leads to cell death, we initially evaluated whether the disruption of *Mpeg1* protects the cells from the cytotoxic effects of saporin and other cytosolic toxins. We incubated control and *Mpeg1*$^{KO}$ MutuDCs with saporin for 24 h and quantified surviving cells by flow cytometry. Indeed, Mpeg1$^{KO}$ MutuDCs were more resistant to saporin-mediated cell death, and we observed similar levels of protection from death induced by a different RIP, gelonin (Fig. 3B). Importantly, the KO cells were not protected against cell death initiated by molecules that do not need to access the cytosol or against membrane permeable agents which can enter the cytosol freely. For example, knocking out *Mpeg1* conferred no resistance to Poly (I:C), which in cDC1s induces cell death via endosomal Toll like receptor 3, Tlr3 (*21*) or to cycloheximide, a membrane-permeable translation inhibitor (Fig. 3B). We also tested the sensitivity of Mpeg1$^{KO}$ DCs to a glycopeptide chemotherapeutic, bleomycin A2, which induces DNA damage, but due to its hydrophilicity does not enter the cells efficiently (*32*). We used automated imaging to monitor the growth rate of NT and *Mpeg1*$^{KO}$ MutuDC cultured in the presence of increasing

concentrations of bleomycin and observed that loss of perforin-2 renders MutuDCs more resistant to bleomycin-mediated cytotoxicity (Fig. 3B).

We went on to verify that the observed sensitivity of perforin-2-expressing DCs to cytosolic toxins is due to an efficient escape pathway rather than due to inefficient uptake (Fig. 3C). In the saporin-puromycin assay with Atto 550-labelled saporin, endocytic escape was impaired in the *Mpeg1*$^{KO}$ DCs, even though NT and KO cells internalised similar amounts of fluorescent saporin (Fig. 3C). We could also rescue saporin import without affecting uptake by transducing *Mpeg1*$^{KO}$ cells with lentiviruses expressing full length sgRNA-resistant *Mpeg1* (Fig. 3D and fig. S2C).

Finally, we addressed whether the pore-forming ability of perforin-2 is required for endocytic escape. Perforin-2 forms pores by oligomerisation and unwinding of two helices in the MACPF domain into β sheets (indicated in red in Fig. 3A) (*28*, *29*). To test whether this conformational change is required for perforin-2 activity in DCs, we generated two mutants: *Mpeg1*$^{G212V/A213V}$ with mutations in the conserved MACPF motif (*33*) and *Mpeg1*$^{K251C/G286C}$, where we introduced a disulphide bond previously shown to constrain one of the pore-forming helices preventing pore formation *in vitro* (*28*). Both, *Mpeg1*$^{G212V/A213V}$ and *Mpeg1*$^{K251C/G286C}$, were expressed at similar levels to Mpeg1$^{WT}$, but neither rescued saporin escape in *Mpeg1*$^{KO}$ MutuDCs (Fig. 3E and fig. S2D). Altogether, these data suggest that perforin-2 pores mediate endocytic escape in cross-presenting DCs.

**Perforin-2 is sufficient for endocytic escape in non-immune cells**

Since perforin-2 is restricted to antigen presenting cells (*25*, *34*), we asked whether it is sufficient to drive endocytic escape in non-immune cells. To this end, we generated HEK293Ts and HeLa cells expressing either murine *Mpeg1* together with a fluorescent protein (*mScarlet or BFP),* or the fluorescent protein alone, and used them in a range of endocytic escape assays. Indeed, ectopic expression of perforin-2 was sufficient to promote saporin escape in HEK293Ts (Fig. 4A).

We also monitored endocytic escape of β-lactamase using a previously described flow cytometry-based assay (*35*, *36*). Here, the cells are first loaded with a cytosolic dye CCF4 consisting of fluorescein and 7-hydroxycoumarin linked via a β-lactam ring. Escape of β-lactamase into the cytosol results in cleavage of a β-lactam ring and a shift in CCF4 fluorescence from green to blue. We pulsed the cells with β-lactamase for different amounts of time and monitored the proportion of cells with cleaved CCF4 by flow cytometry. Expression of perforin-2 increased the frequency of cells with cleaved CCF4 and thus the efficiency of β-lactamase escape in HeLa cells (Fig. 4B and fig. S3B). We then adopted a recently reported split luciferase assay to monitor endocytic escape of recombinant microtubule-associated protein, tau(*37*). We expressed a large 18 kDa NanoLuc subunit (LgBiT) in the cytosol of control and perforin-2-expressing HEK293Ts and pulsed the cells with oligomers of recombinant tau fused with a high-affinity 11 amino acid-long HiBit peptide. Upon entry into the cytosol, HiBiT binds LgBiT resulting in catalytic activity of luciferase and luminescence in the presence of the enzymatic substrate, Nano-Glo$^{(R)}$. Again, in perforin-2-expressing HEK293Ts, tau-HiBit escape was more efficient compared to the control line (Fig. 4C). Finally, we used the bleomycin-sensitivity assay described above to demonstrate that expression

195 of perforin-2 renders HeLa cells more sensitive to bleomycin-mediated toxicity (Fig. 4D). Collectively, these data show that ectopic expression of perforin-2 is sufficient to drive endocytic escape in non-immune cells.

**Proteolytic cleavage releases the pore-forming domain of perforin-2**

Given the cytotoxic potential of pore-forming proteins, we asked how cDC1s regulate pore-
200 formation and restrict it to antigen containing compartments (36, 37).

Perforin-2 is the only known mammalian pore-forming protein with an additional transmembrane domain (TMD) not involved in pore formation (see Fig. 3A). The TMD has been proposed to act as an anchor preventing damage to endogenous membranes and orientating the pore towards intravacuolar bacteria residing in phagosomes (27, 28). We hypothesised that
205 perforin-2 is activated by proteolytic release of the ectodomain in late endocytic compartments. This hypothesis initially emerged from analysis of SILAC-based organellar mapping data which we generated in a previous study (*20*). The organellar maps were prepared by mass spectrometry-based analysis of the fractionated post-nuclear supernatants from control cells and cells treated with drugs that promoted lysosomal leakiness, Prazosin and Tamoxifen (fig. S4)
210 (*38*). In the original maps, perforin-2 had a profile similar to lysosomal proteins. Here, instead of analysing protein profiles, we analysed each tryptic peptide individually, only including endo- or lysosomal proteins (Fig. 5A). We confirmed clustering of individual peptides derived from endosome- or lysosome-resident proteins and of peptides derived from transmembrane or luminal proteins in the lysosome cluster. 15 out of 17 perforin-2-derived peptides clustered with soluble
215 rather than transmembrane lysosomal proteins suggesting that the perforin-2 ectodomain is released from the TMD anchor. The remaining peptides, p340-372 (within the EGF domain) and p629-635 (within a region proximal to the TMD), co-clustered with endosomal proteins (such as Vps35, Fig. 5A) suggesting that they are present in the full-length protein transiting through endosomes but are absent (cleaved) once perforin-2 reaches acidic compartments.

220 To confirm that perforin-2 is cleaved near the TMD and within the EGF domain, we probed MutuDC lysates with domain-specific antibodies (Fig. 5C). All of the antibodies (αMACPF, αP2 and the αC-terminal tail) detected full length perforin-2 at 70 kDa. We also detected a 40 kDa band with the αMACPF Ab and a 25 kDa band with the αP2 Ab consistent with the cleavage in the EGF domain. The antibody against the C-terminal tail detected only full-length protein,
225 suggesting that the tail (and most likely the TMD) are rapidly degraded following release of the ectodomain. To test whether this proteolytic processing takes place in lysosomes, we immunostained MutuDCs with the αC-term antibody, and identified full-length perforin-2 in a Vps35+ compartment, but not in Lysotracker-labelled lysosomes (Fig. 5D). In contrast, the αMACPF antibody colocalised with lysotracker, but not with Vps35, suggesting that either the Ab
230 recognises primarily mature perforin-2 or that the majority of the protein is in lysosomes at steady-state. Together, these data suggested that full length perforin-2 resides in (or transits through) endosomes, and upon reaching low pH compartments, it undergoes maturation involving two cleavage events.

To test whether perforin-2 maturation is indeed pH dependent, we used Bafilomycin A1 (BafA1),
235 a V-ATPase inhibitor that interferes with lysosomal acidification (*39*). In BafA1-treated MutuDCs, perforin-2 accumulated as a 70 kDa protein while the 40 kDa MACPF fragment was no longer detected (Fig. 5E). To validate the position of the two putative cleavage sites, we performed a comparative proteomics analysis of tryptic and semi-tryptic perforin-2 peptides from control and BafA1-treated cells (Fig. 5F and table S2). Semi-tryptic peptides are considered to be derived
240 from proteins that were cleaved in the cell, prior to sample processing. Semi-tryptic peptide p340-349 was significantly depleted in BafA1-treated cells (Fig. 5F) consistent with a pH-dependent cleavage between the MACPF and P2. We were also able to reconstitute this cleavage event *in vitro* with asparagine endopeptidase, AEP (fig. S5A and B). Furthermore, tryptic peptides p621-628 and p629-637 were significantly enriched in BafA1-treated cells consistent with the model
245 where TMD-containing C-terminal portion of perforin-2 is lost upon reaching acidic compartments.

In summary, these experiments reveal that perforin-2 activity is controlled by at least two cleavage events. The cleavage in the TMD-proximal CTT domain releases the ectodomain into the lysosomal lumen and is necessary to orient the pore-forming domain towards the endogenous
250 membranes. The cleavage in the EGF domain is not required for pore formation *in vitro* (*28*, *40*), but may provide additional flexibility to complete pore insertion *in vivo* or may serve to inactivate the pores.

**Perforin-2 undergoes processing in antigen-containing compartments**

To demonstrate that perforin-2 undergoes maturation in antigen-containing compartments, we
255 analysed perforin-2 recruitment to phagosomes by phagoFACS (*41*). MutuDCs were pulsed with 3 µm ovalbumin-coated polystyrene beads (OVA-beads) for 25 min at 16°C, followed by 5 min at 37°C (Fig. 6A) and the non-internalised beads were then washed away. At different time points, we disrupted the cells to release phagosomes, stained them and analysed by flow cytometry. Neither the rate of Lamp1 acquisition nor that of ovalbumin degradation was affected by
260 knocking out *Mpeg1* suggesting perforin-2 does not regulate phagosome maturation (fig. S6B and C). Using the perforin-2 αC-term antibody (Fig. 6B), we demonstrated that perforin-2 was rapidly recruited to phagosomes reaching its highest levels within 30 min after phagosome formation. This rapid acquisition suggests that perforin-2 is recruited prior to phagosome-lysosome fusion (*42*). Indeed, we could inhibit perforin-2 recruitment with an inhibitor of ARF GTPases Brefeldin
265 A (BFA), which blocks protein trafficking through the early secretory pathway, suggesting perforin-2 is delivered to phagosomes from the Golgi. In phagoFACS experiments with the αMACPF Ab, perforin-2 acquisition was also BFA-dependent (Fig 6B and C). Unlike with the αC-term Ab, the αMACPF staining was restricted to mature, Lamp1+ phagosomes and increased over time while the signal for the cytosolic tail was gradually lost (Fig. 6C). Taken together, these data
270 indicate that the C-terminal part of perforin-2 is cleaved off and degraded during phagosome maturation, while the ectodomain undergoes a conformational change in mature phagosomes, which exposes an epitope recognised by the αMACPF antibody.

Finally, to confirm that perforin-2 contributes to the escape of phagocytic cargo, we conjugated saporin or BSA via thiol-ester bonds to OVA-beads and used them in the saporin-puromycin assay (Fig. 6D). We pulsed WT and *Mpeg1*$^{KO}$ MutuDC with the beads and incubated them at 37°C for 5 hours. In WT, but not in *Mpeg1*$^{KO}$ MutuDCs, saporin was able to escape from phagosomes leading to translation arrest (Fig. 6E).

**Perforin-2 is expressed in antigen-presenting cells and facilitates cross-presentation**

To test whether the perforin-2-mediated endocytic escape pathway is involved in the delivery of antigens for cross-presentation, we generated knockout mice in which we disrupted the *Mpeg1* gene using a CRISPR-based approach (fig. S7A and B). Notably, knocking out *Mpeg1* did not result in any obvious disease phenotype. Furthermore, *Mpeg1*$^{-/-}$ mice had immune cell frequencies comparable to WT mice (ffigig. S7C and D). Using intracellular staining, we confirmed that perforin-2 is expressed in spleen-resident cDC1s (Lin$^{-}$CD11c$^{+}$CX$_{3}$CR1$^{-}$XCR1$^{+}$) but not in spleen-resident cDC2s (Lin$^{-}$CD11c$^{+}$CX$_{3}$CR1$^{-}$CD172a$^{+}$), T cells, B cells or NK cells (fig. S8A). Interestingly, we also detected perforin-2 in other cell types, previously shown to cross-present *in vivo*, including splenic macropahges, plasmacytoid DC (pDCs), and a subpopulation of migratory cDC2s (Lin$^{-}$CD11c$^{+}$CX$_{3}$CR1$^{+}$CD172a$^{+}$) (*43–45*) (Fig. 7A and fig. S8A). Indeed, splenic macrophages and pDCs, efficiently imported saporin into the cytosol *ex vivo* (fig. S8B and C). To confirm that loss of perforin-2 results in defective endocytic escape in primary cells, we performed the saporin-puromycin assay in bone marrow-derived DCs generated from WT and Mpeg1$^{-/-}$ mice using Flt3-L and GM-CSF (Fig. 7B). In the BMDC$^{Flt3L/GM-CSF}$ cultures, both cDC1s (CD11c$^{+}$ XCR1$^{+}$) and a large proportion of cDC2s (CD11c$^{+}$ CD172a$^{+}$) express perforin-2 (Fig. 7B). Saporin import into the cytosol is perforin-2-dependent in both subsets, as indicated by the differences in puromycin incorporation (Fig. 7C).

Finally, we asked whether perforin-2 mediated endocytic escape delivers antigens for cross-presentation. To assess the efficiency of antigen presentation *in vivo*, we adoptively transferred OT-I T cells expressing a TCR specific to ovalbumin peptide 257-264 displayed on H2Kb molecules and monitored OT-I proliferation following immunisation. Since cross-presentation of soluble ovalbumin, which can be processed by cell types other than cDC1s (*44*, *46*), was not significantly affected in the Mpeg1-/- mice (fig. S8F), we used dead cells as an antigen source. As anticipated, Mpeg1-/- had fewer OT-I T cells following immunisation with UVC-irradiated 3T3 fibroblasts coated with ovalbumin compared to WT mice. Thus, loss of perforin-2 leads to a defect in cross-presentation of cell associated antigens in vivo (Fig. 7D and E), suggesting that in cross-presenting cells, endocytic pores provide a route for cytosolic entry of antigens.

## Conclusions

In this study, we uncover a mechanism of endocytic escape that is governed by a cell type-specific pore-forming effector protein, perforin-2. The role of perforin-2 in the delivery of antigens for cross-presentation suggests that the immune system evolved to employ two related pore-forming effectors, perforin-1 and perforin-2, during different stages of adaptive immune responses. Perforin-1, expressed by cytotoxic T cells, is a well characterised effector employed for the delivery of granzymes into the cytosol of target cells (*47*). Our data, suggest that perforin-2 delivers endocytic contents into the cytosol of cross-presenting DCs, to enable the generation of MHC-I:peptide complexes for stimulation of naïve T cells.

We do not exclude the possibility that in different contexts, membrane destabilisation may also act to effectively deliver antigens for cross-presentation (*48*). Membrane integrity is regulated by a wide range of proteins involved in cell homeostasis (*49*, *50*), and as a result, different perturbations can result in leakage of endosomal contents into the cytosol under pathological conditions. Nevertheless, considering the restricted expression of *Mpeg1* to subsets of professional antigen presenting cells, our data points to at an important role of perforin-2 during the initiation of immune responses. The ability to genetically manipulate perforin-2-mediated endocytic escape also provides a new tool to explore the contribution of the escape pathway to anti-cancer and anti-viral immune responses *in vivo*.

## References


1. M. J. Palmowski, U. Gileadi, M. Salio, A. Gallimore, M. Millrain, E. James, C. Addey, D. Scott, J. Dyson, E. Simpson, V. Cerundolo, Role of Immunoproteasomes in Cross-Presentation. *J Immunol*. 177, 983–990 (2006).

2. J. Helft, B. Manicassamy, P. Guermonprez, D. Hashimoto, A. Silvin, J. Agudo, B. D. Brown, M. Schmolke, J. C. Miller, M. Leboeuf, K. M. Murphy, A. García-Sastre, M. Merad, Cross-presenting CD103+ dendritic cells are protected from influenza virus infection. *J Clin Invest*. 122, 4037–4047 (2012).

3. D. J. Theisen, J. T. Davidson, C. G. Briseño, M. Gargaro, E. J. Lauron, Q. Wang, P. Desai, V. Durai, P. Bagadia, J. R. Brickner, W. L. Beatty, H. W. Virgin, W. E. Gillanders, N. Mosammaparast, M. S. Diamond, L. D. Sibley, W. Yokoyama, R. D. Schreiber, T. L. Murphy, K. M. Murphy, WDFY4 is required for cross-presentation in response to viral and tumor antigens. *Science*. 362, 694–699 (2018).

4. E. Giampazolias, O. Schulz, K. H. J. Lim, N. C. Rogers, P. Chakravarty, N. Srinivasan, O. Gordon, A. Cardoso, M. D. Buck, E. Z. Poirier, J. Canton, S. Zelenay, S. Sammicheli, N. Moncaut, S. Varsani-Brown, I. Rosewell, C. R. e Sousa, Secreted gelsolin inhibits DNGR-1-dependent cross-presentation and cancer immunity. *Cell*. 184, 4016-4031.e22 (2021).

5. M. Kovacsovics-Bankowski, K. L. Rock, A Phagosome-to-Cytosol Pathway for Exogenous Antigens Presented on MHC Class I Molecules. *Science*. 267, 243–246 (1995).

6. J. Canton, H. Blees, C. M. Henry, M. D. Buck, O. Schulz, N. C. Rogers, E. Childs, S. Zelenay, H. Rhys, M.-C. Domart, L. Collinson, A. Alloatti, C. J. Ellison, S. Amigorena, V. Papayannopoulos, D. C. Thomas, F. Randow, C. R. E. Sousa, The receptor DNGR-1 signals for phagosomal rupture to promote cross-presentation of dead-cell-associated antigens. *Nat Immunol*. 22, 140–153 (2020).

7. M. Zehner, A. L. Marschall, E. Bos, J.-G. Schloetel, C. Kreer, D. Fehrenschild, A. Limmer, F. Ossendorp, T. Lang, A. J. Koster, S. Dübel, S. Burgdorf, The translocon protein Sec61 mediates antigen transport from endosomes in the cytosol for cross-presentation to CD8(+) T cells. *Immunity*. 42, 850–63 (2015).

8. M. Zehner, A. I. Chasan, V. Schuette, M. Embgenbroich, T. Quast, W. Kolanus, S. Burgdorf, Mannose receptor polyubiquitination regulates endosomal recruitment of p97 and cytosolic antigen translocation for cross-presentation. *Proc National Acad Sci*. 108, 9933–9938 (2011).

9. I. Dingjan, D. R. Verboogen, L. M. Paardekooper, N. H. Revelo, S. P. Sittig, L. J. Visser, G. F. von Mollard, S. S. Henriet, C. G. Figdor, M. ter Beest, G. van den Bogaart, Lipid peroxidation causes endosomal antigen release for cross-presentation. *Sci Rep-uk*. 6, 22064 (2016).

10. S. C. Nalle, R. B. da Silva, H. Zhang, M. Decker, C. Chalouni, M. Xu, G. Posthuma, A. de Mazière, J. Klumperman, A. B. Morelli, S. J. Fleire, A. S. Verkman, E. S. Trombetta, M. L. Albert, I. Mellman, Aquaporin-3 regulates endosome-to-cytosol transfer via lipid peroxidation for cross presentation. *Plos One*. 15, e0238484 (2020).

11. Y. Ding, Z. Guo, Y. Liu, X. Li, Q. Zhang, X. Xu, Y. Gu, Y. Zhang, D. Zhao, X. Cao, The lectin Siglec-G inhibits dendritic cell cross-presentation by impairing MHC class I–peptide complex formation. *Nat Immunol*. 17, 1167–1175 (2016).

12. J. Canton, H. Blees, C. M. Henry, M. D. Buck, O. Schulz, N. C. Rogers, E. Childs, S. Zelenay, H. Rhys, M.-C. Domart, L. Collinson, A. Alloatti, C. J. Ellison, S. Amigorena, V. Papayannopoulos, D. C. Thomas, F. Randow, C. R. e Sousa, The receptor DNGR-1 signals for phagosomal rupture to promote cross-presentation of dead-cell-associated antigens. *Nat Immunol*. 22, 1–14 (2020).

13. S. Zelenay, A. M. Keller, P. G. Whitney, B. U. Schraml, S. Deddouche, N. C. Rogers, O. Schulz, D. Sancho, C. R. e Sousa, The dendritic cell receptor DNGR-1 controls endocytic handling of necrotic cell antigens to favor cross-priming of CTLs in virus-infected mice. *The Journal of clinical investigation*. 122, 1615–1627 (2012).

14. K. Nielsen, R. S. Boston, R IBOSOME -I NACTIVATING P ROTEINS□: A Plant Perspective. *Annu Rev Plant Phys*. 52, 785–816 (2001).

15. E. K. Schmidt, G. Clavarino, M. Ceppi, P. Pierre, SUnSET, a nonradioactive method to monitor protein synthesis. *Nature Methods*. 6, 275–277 (2009).

16. A. Dalet, R. J. Argüello, A. Combes, L. Spinelli, S. Jaeger, M. Fallet, T. P. V. Manh, A. Mendes, J. Perego, M. Reverendo, V. Camosseto, M. Dalod, T. Weil, M. A. Santos, E. Gatti, P. Pierre, Protein synthesis inhibition and GADD34 control IFN□β heterogeneous expression in response to dsRNA. *The EMBO Journal*. 36, 761–782 (2017).

17. M. B. Yarmolinsky, G. L. D. L. Haba, INHIBITION BY PUROMYCIN OF AMINO ACID INCORPORATION INTO PROTEIN*. *Proc National Acad Sci*. 45, 1721–1729 (1959).

18. K. Hildner, B. T. Edelson, W. E. Purtha, M. Diamond, H. Matsushita, M. Kohyama, B. Calderon, B. U. Schraml, E. R. Unanue, M. S. Diamond, R. D. Schreiber, T. L. Murphy, K. M. Murphy, Batf3 deficiency reveals a critical role for CD8alpha+ dendritic cells in cytotoxic T cell immunity. *Sci New York N Y*. 322, 1097–100 (2008).

19. M. L. Lin, Y. Zhan, A. I. Proietto, S. Prato, L. Wu, W. R. Heath, J. A. Villadangos, A. M. Lew, Selective suicide of cross-presenting CD8+ dendritic cells by cytochrome c injection shows functional heterogeneity within this subset. *P Natl Acad Sci Usa*. 105, 3029–34 (2008).

20. P. Kozik, M. Gros, D. N. Itzhak, L. Joannas, S. Heurtebise-Chrétien, P. A. Krawczyk, P. Rodríguez-Silvestre, A. Alloatti, J. G. Magalhaes, E. D. Nery, G. H. H. Borner, S. Amigorena, Small Molecule Enhancers of Endosome-to-Cytosol Import Augment Anti-tumor Immunity. *Cell Reports*. 32, 107905 (2020).

21. S. A. F. Marraco, F. Grosjean, A. Duval, M. Rosa, C. Lavanchy, D. Ashok, S. Haller, L. A. Otten, Q.-G. Steiner, P. Descombes, C. A. Luber, F. Meissner, M. Mann, L. Szeles, W. Reith, H. Acha-Orbea, Novel murine dendritic cell lines: a powerful auxiliary tool for dendritic cell research. *Front Immunol*. 3, 331 (2012).

22. B. E. Steinberg, K. K. Huynh, A. Brodovitch, S. Jabs, T. Stauber, T. J. Jentsch, S. Grinstein, A cation counterflux supports lysosomal acidification. *J Cell Biol*. 189, 1171–1186 (2010).

23. M. Gros, E. Segura, D. C. Rookhuizen, B. Baudon, S. Heurtebise-Chrétien, N. Burgdorf, M. Maurin, E. A. Kapp, R. J. Simpson, P. Kozik, J. A. Villadangos, M. J. M. Bertrand, M. Burbage, S. Amigorena, Endocytic membrane repair by ESCRT-III controls antigen export to the cytosol during antigen cross-presentation. *Cell Reports*. 40, 111205 (2022).

24. A. J. Monteith, S. Kang, E. Scott, K. Hillman, Z. Rajfur, K. Jacobson, M. J. Costello, B. J. Vilen, Defects in lysosomal maturation facilitate the activation of innate sensors in systemic lupus erythematosus. *Proceedings of the National Academy of Sciences*. 113, E2142-51 (2016).

25. T. I. G. P. Consortium, T. S. P. Heng, M. W. Painter, K. Elpek, V. Lukacs-Kornek, N. Mauermann, S. J. Turley, D. Koller, F. S. Kim, A. J. Wagers, N. Asinovski, S. Davis, M. Fassett, M. Feuerer, D. H. D. Gray, S. Haxhinasto, J. A. Hill, G. Hyatt, C. Laplace, K. Leatherbee, D. Mathis, C. Benoist, R. Jianu, D. H. Laidlaw, J. A. Best, J. Knell, A. W. Goldrath, J. Jarjoura, J. C. Sun, Y. Zhu, L. L. Lanier, A. Ergun, Z. Li, J. J. Collins, S. A. Shinton, R. R. Hardy, R. Friedline, K. Sylvia, J. Kang, The Immunological Genome Project: networks of gene expression in immune cells. *Nat Immunol*. 9, 1091–1094 (2008).

26. D. Sichien, C. L. Scott, L. Martens, M. Vanderkerken, S. Van Gassen, M. Plantinga, T. Joeris, S. De Prijck, L. Vanhoutte, M. Vanheerswynghels, G. Van Isterdael, W. Toussaint, F. B. Madeira, K. Vergote, W. W. Agace, B. E. Clausen, H. Hammad, M. Dalod, Y. Saeys, B. N. Lambrecht, M. Guilliams, IRF8 Transcription Factor Controls Survival and Function of Terminally Differentiated Conventional and Plasmacytoid Dendritic Cells, Respectively. *Immunity*. 45, 626–640 (2016).

27. R. McCormack, L. R. de Armas, M. Shiratsuchi, J. E. Ramos, E. R. Podack, Inhibition of intracellular bacterial replication in fibroblasts is dependent on the perforin-like protein (perforin-2) encoded by macrophage-expressed gene 1. *J Innate Immun*. 5, 185–94 (2012).

28. T. Ni, F. Jiao, X. Yu, S. Aden, L. Ginger, S. I. Williams, F. Bai, V. Pražák, D. Karia, P. Stansfeld, P. Zhang, G. Munson, G. Anderluh, S. Scheuring, R. J. C. Gilbert, Structure and mechanism of bactericidal mammalian perforin-2, an ancient agent of innate immunity. *Sci Adv*. 6, eaax8286 (2020).

29. S. S. Pang, C. Bayly-Jones, M. Radjainia, B. A. Spicer, R. H. P. Law, A. W. Hodel, E. S. Parsons, S. M. Ekkel, P. J. Conroy, G. Ramm, H. Venugopal, P. I. Bird, B. W. Hoogenboom, I. Voskoboinik, Y. Gambin, E. Sierecki, M. A. Dunstone, J. C. Whisstock, The cryo-EM structure of the acid activatable pore-forming immune effector Macrophage-expressed gene 1. *Nat Commun*. 10, 4288 (2019).

30. R. M. McCormack, L. R. de Armas, M. Shiratsuchi, D. G. Fiorentino, M. L. Olsson, M. G. Lichtenheld, A. Morales, K. Lyapichev, L. E. Gonzalez, N. Strbo, N. Sukumar, O. Stojadinovic, G. V. Plano, G. P. Munson, M. Tomic-Canic, R. S. Kirsner, D. G. Russell, E. R. Podack, Perforin-2 is essential for intracellular defense of parenchymal cells and phagocytes against pathogenic bacteria. *Elife*. 4, e06508 (2015).

31. S. Ebrahimnezhaddarzi, C. H. Bird, C. C. Allison, D. E. Tuipulotu, X. Kostoulias, C. Macri, M. D. Stutz, G. Abraham, D. Kaiserman, S. S. Pang, S. M. Man, J. D. Mintern, T. Naderer, A. Y. Peleg, M. Pellegrini, J. C. Whisstock, P. I. Bird, Mpeg1 is not essential for anti□bacterial or anti□viral immunity, but is implicated in antigen presentation. *Immunol Cell Biol* (2022), doi:10.1111/imcb.12554.

32. M. J. Jaroszeski, V. Dang, C. Pottinger, J. Hickey, R. Gilbert, R. Heller, Toxicity of anticancer agents mediated by electroporation in vitro. *Anti-cancer Drug*. 11, 201–208 (2000).

33. C. J. Rosado, A. M. Buckle, R. H. P. Law, R. E. Butcher, W.-T. Kan, C. H. Bird, K. Ung, K. A. Browne, K. Baran, T. A. Bashtannyk-Puhalovich, N. G. Faux, W. Wong, C. J. Porter, R. N. Pike, A. M. Ellisdon, M. C. Pearce, S. P. Bottomley, J. Emsley, A. I. Smith, J. Rossjohn, E. L. Hartland, I. Voskoboinik, J. A. Trapani, P. I. Bird, M. A. Dunstone, J. C. Whisstock, A Common Fold Mediates Vertebrate Defense and Bacterial Attack. *Science*. 317, 1548–1551 (2007).

34. J. Lonsdale, J. Thomas, M. Salvatore, R. Phillips, E. Lo, S. Shad, R. Hasz, G. Walters, F. Garcia, N. Young, B. Foster, M. Moser, E. Karasik, B. Gillard, K. Ramsey, S. Sullivan, J. Bridge, H. Magazine, J. Syron, J. Fleming, L. Siminoff, H. Traino, M. Mosavel, L. Barker, S. Jewell, D. Rohrer, D. Maxim, D. Filkins, P. Harbach, E. Cortadillo, B. Berghuis, L. Turner, E. Hudson, K. Feenstra, L. Sobin, J. Robb, P. Branton, G. Korzeniewski, C. Shive, D. Tabor, L. Qi, K. Groch, S. Nampally, S. Buia, A. Zimmerman, A. Smith, R. Burges, K. Robinson, K. Valentino, D. Bradbury, M. Cosentino, N. Diaz-Mayoral, M. Kennedy, T. Engel, P. Williams, K. Erickson, K. Ardlie, W. Winckler, G. Getz, D. DeLuca, D. MacArthur, M. Kellis, A. Thomson, T. Young, E. Gelfand, M. Donovan, Y. Meng, G. Grant, D. Mash, Y. Marcus, M. Basile, J. Liu, J. Zhu, Z. Tu, N. J. Cox, D. L. Nicolae, E. R. Gamazon, H. K. Im, A. Konkashbaev, J. Pritchard, M. Stevens, T. Flutre, X. Wen, E. T. Dermitzakis, T. Lappalainen, R. Guigo, J. Monlong, M. Sammeth, D. Koller, A. Battle, S. Mostafavi, M. McCarthy, M. Rivas, J. Maller, I. Rusyn, A. Nobel, F. Wright, A. Shabalin, M. Feolo, N. Sharopova, A. Sturcke, J. Paschal, J. M. Anderson, E. L. Wilder, L. K. Derr, E. D. Green, J. P. Struewing, G. Temple, S. Volpi, J. T. Boyer, E. J. Thomson, M. S. Guyer, C. Ng, A. Abdallah, D. Colantuoni, T. R. Insel, S. E. Koester, A. R. Little, P. K. Bender, T. Lehner, Y. Yao, C. C. Compton, J. B. Vaught, S. Sawyer, N. C. Lockhart, J. Demchok, H. F. Moore, The Genotype-Tissue Expression (GTEx) project. *Nat Genet*. 45, 580–585 (2013).

35. I. Cebrian, G. Visentin, N. Blanchard, M. Jouve, A. Bobard, C. Moita, J. Enninga, L. F. Moita, S. Amigorena, A. Savina, Sec22b Regulates Phagosomal Maturation and Antigen Crosspresentation by Dendritic Cells. *Cell*. 147, 1355–1368 (2011).

36. P. Kozik, M. Gros, D. N. Itzhak, L. Joannas, S. Heurtebise-Chrétien, P. A. Krawczyk, P. Rodríguez-Silvestre, A. Alloatti, J. G. Magalhaes, E. D. Nery, G. H. H. Borner, S. Amigorena, Small Molecule Enhancers of Endosome-to-Cytosol Import Augment Anti-tumor Immunity. *Cell Reports*. 32, 107905 (2020).

37. B. J. Tuck, L. V. C. Miller, T. Katsinelos, A. E. Smith, E. L. Wilson, S. Keeling, S. Cheng, M. J. Vaysburd, C. Knox, L. Tredgett, E. Metzakopian, L. C. James, W. A. McEwan, Cholesterol determines the cytosolic entry and seeded aggregation of tau. *Cell Reports*. 39, 110776 (2022).

38. D. N. Itzhak, S. Tyanova, J. Cox, G. H. Borner, Global, quantitative and dynamic mapping of protein subcellular localization. *Elife*. 5, e16950 (2016).

39. R. Wang, J. Wang, A. Hassan, C.-H. Lee, X.-S. Xie, X. Li, Molecular basis of V-ATPase inhibition by bafilomycin A1. *Nat Commun*. 12, 1782 (2021).

40. F. Jiao, F. Dehez, T. Ni, X. Yu, J. S. Dittman, R. Gilbert, C. Chipot, S. Scheuring, Perforin-2 clockwise hand-over-hand pre-pore to pore transition mechanism. *Nat Commun*. 13, 5039 (2022).

41. E. Hoffmann, F. Kotsias, G. Visentin, P. Bruhns, A. Savina, S. Amigorena, Autonomous phagosomal degradation and antigen presentation in dendritic cells. *P Natl Acad Sci Usa*. 109, 14556–61 (2012).

42. F. M. Cruz, J. D. Colbert, K. L. Rock, The GTPase Rab39a promotes phagosome maturation into MHC□I antigen□presenting compartments. *Embo J*. 39, e102020 (2020).

43. C. Bosteels, K. Neyt, M. Vanheerswynghels, M. J. van Helden, D. Sichien, N. Debeuf, S. D. Prijck, V. Bosteels, N. Vandamme, L. Martens, Y. Saeys, E. Louagie, M. Lesage, D. L. Williams, S.-C. Tang, J. U. Mayer, F. Ronchese, C. L. Scott, H. Hammad, M. Guilliams, B. N. Lambrecht, Inflammatory Type 2 cDCs Acquire Features of cDC1s and Macrophages to Orchestrate Immunity to Respiratory Virus Infection. *Immunity*. 52, 1039-1056.e9 (2020).

44. M. Enders, L. Franken, M.-S. Philipp, N. Kessler, A.-K. Baumgart, M. Eichler, E. J. H. Wiertz, N. Garbi, C. Kurts, Splenic Red Pulp Macrophages Cross-Prime Early Effector CTL That Provide Rapid Defense against Viral Infections. *J Immunol Baltim Md 1950*. 204, 87–100 (2019).

45. M. Oberkampf, C. Guillerey, J. Mouriès, P. Rosenbaum, C. Fayolle, A. Bobard, A. Savina, E. Ogier-Denis, J. Enninga, S. Amigorena, C. Leclerc, G. Dadaglio, Mitochondrial reactive oxygen species regulate the induction of CD8+ T cells by plasmacytoid dendritic cells. *Nat Commun*. 9, 2241 (2018).

46. N. M. Kretzer, D. J. Theisen, R. Tussiwand, C. G. Briseño, G. E. Grajales-Reyes, X. Wu, V. Durai, J. Albring, P. Bagadia, T. L. Murphy, K. M. Murphy, RAB43 facilitates cross-presentation of cell-associated antigens by CD8α+ dendritic cells. *J Exp Med*. 213, 2871–2883 (2016).

47. I. Voskoboinik, J. C. Whisstock, J. A. Trapani, Perforin and granzymes: function, dysfunction and human pathology. *Nat Rev Immunol*. 15, 388–400 (2015).

48. P. Cresswell, A personal retrospective on the mechanisms of antigen processing. *Immunogenetics*. 71, 141–160 (2019).

49. M. L. Skowyra, P. H. Schlesinger, T. V. Naismith, P. I. Hanson, Triggered recruitment of ESCRT machinery promotes endolysosomal repair. *Science*. 360, eaar5078 (2018).

50. I. Maejima, A. Takahashi, H. Omori, T. Kimura, Y. Takabatake, T. Saitoh, A. Yamamoto, M. Hamasaki, T. Noda, Y. Isaka, T. Yoshimori, Autophagy sequesters damaged lysosomes to control lysosomal biogenesis and kidney injury. *Embo J*. 32, 2336–2347 (2013).

51. P. Kozik, M. Gros, D. N. Itzhak, L. Joannas, S. Heurtebise-Chrétien, P. A. Krawczyk, P. Rodríguez-Silvestre, A. Alloatti, J. G. Magalhaes, E. D. Nery, G. H. H. Borner, S. Amigorena, Small Molecule Enhancers of Endosome-to-Cytosol Import Augment Anti-tumor Immunity. *Cell Reports*. 32, 107905 (2020).

52. O. Parnas, M. Jovanovic, T. M. Eisenhaure, R. H. Herbst, A. Dixit, C. J. Ye, D. Przybylski, R. J. Platt, I. Tirosh, N. E. Sanjana, O. Shalem, R. Satija, R. Raychowdhury, P. Mertins, S. A. Carr, F. Zhang, N. Hacohen, A. Regev, A Genome-wide CRISPR Screen in Primary Immune Cells to Dissect Regulatory Networks. *Cell*. 162, 675–686 (2015).

53. N. A. Kulak, G. Pichler, I. Paron, N. Nagaraj, M. Mann, Minimal, encapsulated proteomic-sample processing applied to copy-number estimation in eukaryotic cells. *Nat Methods*. 11, 319–24 (2014).

54. J. Cox, M. Mann, MaxQuant enables high peptide identification rates, individualized p.p.b.-range mass accuracies and proteome-wide protein quantification. *Nat Biotechnol*. 26, 1367–72 (2008).

55. J. Cox, M. Y. Hein, C. A. Luber, I. Paron, N. Nagaraj, M. Mann, Accurate proteome-wide label-free quantification by delayed normalization and maximal peptide ratio extraction, termed MaxLFQ. *Mol Cell Proteom Mcp*. 13, 2513–26 (2014).

56. S. Tyanova, T. Temu, P. Sinitcyn, A. Carlson, M. Y. Hein, T. Geiger, M. Mann, J. Cox, The Perseus computational platform for comprehensive analysis of (prote)omics data. *Nat Methods*. 13, 731–740 (2016).

## Acknowledgements

We thank members of the Kozik laboratory for discussions and feedback regarding this work; we also thank G.M. Griffiths and L.C. James for reading of the manuscript and their feedback. We thank N. Hacohen and T. Eisenhauer for their help setting up CRISPR-Cas9 screens. We thank the animal facility/ARES staff, genotyping facility, flow cytometry core and microscopy core at the MRC Laboratory of Molecular Biology for their technical assistance.

## Funding

This work was supported by the UK Medical Research Council (MRC grant no. MC_UP_1201/26).

P.R.-S. was supported by an MRC CellTech Research Fellowship (MRF-104-0007-S-RODRI).

P.A.K. was supported by the Boehringer Ingelheim Fonds PhD Fellowship.

H.H.B. and J.P.S were funded by the Max Planck Society for the Advancement of Science.

A.K.D. received funding from the European Union's Horizon 2020 research and innovation programme under the Marie Sklodowska-Curie grant agreement no. 896725, and a Fellowship from the Alexander von Humboldt Foundation.

B.J.T. was supported by the Cambridge Trust Vice Chancellor Award and Hughes Hall Edwin Leong PhD scholarship.

W.A.M. is a Lister Institute Fellow and supported by a Sir Henry Dale Fellowship jointly funded by the Wellcome Trust and the Royal Society (206248/Z/17/Z). W.A.M. was further supported by the UK Dementia Research Institute which receives its funding from DRI Ltd, funded by the UK Medical Research Council, Alzheimer's Society and Alzheimer's Research UK.

## Author contributions

PRS designed and performed experiments and wrote the manuscript. ML, designed and performed experiments and contributed to the manuscript. AD, JS and GHB carried out mass spectrometry and spatial proteomics analysis. BJT and WAM carried out Tau-HiBit assay. PAK performed experiments and provided scientific insight. PK supervised the study, designed, and performed experiments and wrote the manuscript.

## Additional Information

Correspondence and requests for materials should be addressed to Patrycja Kozik pkozik@mrc-lmb.cam.ac.uk.

## Competing interests

The authors declare no competing interests.

560 **Data and materials availability**

All data are available in the main text or the supplementary materials.

## List of Supplementary Materials

Materials and Methods

Figs. S1 to S8

Table S1

Table S2

Table S3

Table S4

Table S5

References only cited in Supplementary Materials
*52-56*

## Figures

Figure 1

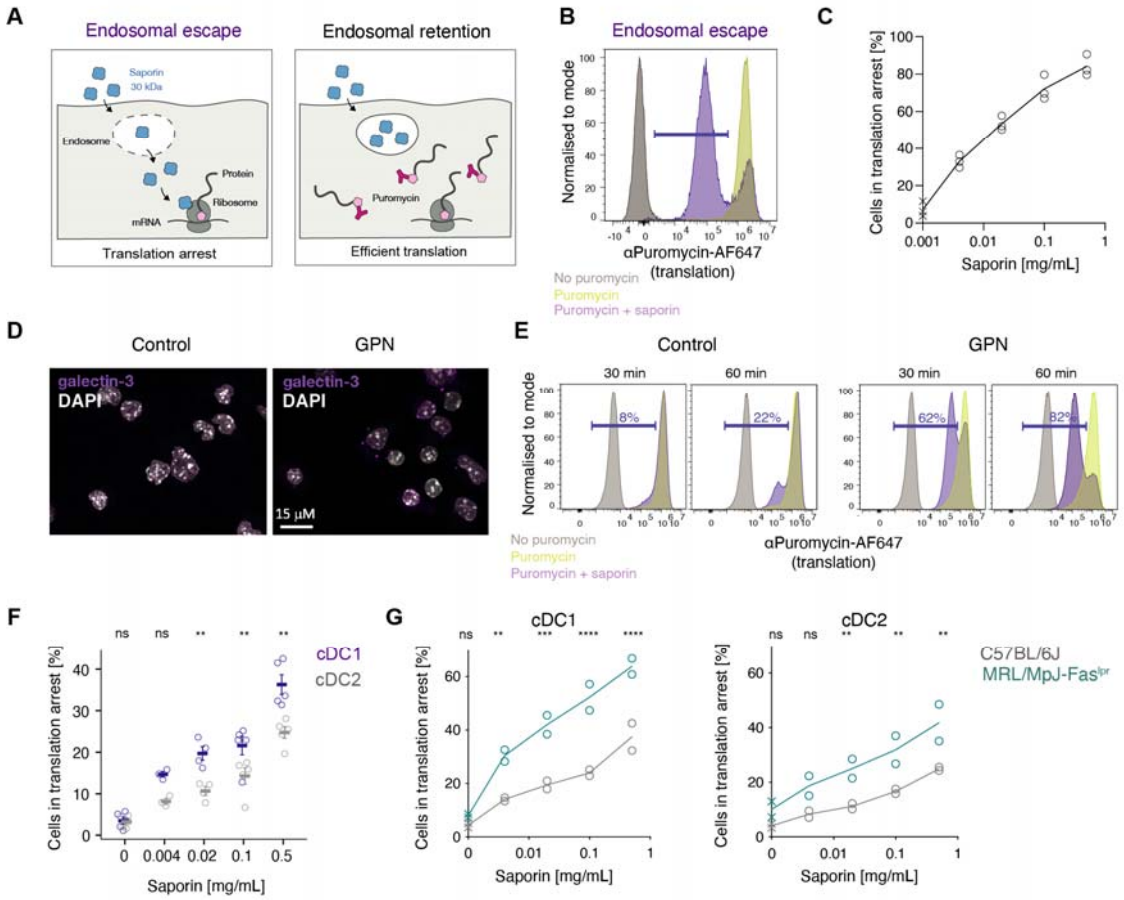


**Fig. 1 Saporin-puromycin assay to monitor endocytic escape in DCs.**

**(A)** Schematic representation of the saporin-puromycin assay. Cells are pulsed with saporin for 2 h and translation is then monitored by labelling nascent polypeptides with puromycin for 30 min. Incorporated puromycin can then be detected with an αPuromycin Ab and flow cytometry. If saporin is retained within the endosomes, translation remains high. When saporin escapes into the cytosol it depurinates ribosomes inducing translation arrest.

**(B)** Representative flow cytometry plot from the saporin-puromycin assay described in (A). MutuDCs were incubated with 0.5 mg/ml of saporin followed by 0.01 mg/mL puromycin (purple histogram), with puromycin alone (yellow) or in media only (grey). Cells in translation arrest are denoted by the purple gate.

**(C)** MutuDCs were incubated with different amounts of saporin as in (B) and the percentage of puromycin$^{low}$ cells quantified by flow cytometry. Data represent three independent experiments. For gating strategy see fig. S1B.

**(D)** Confocal microscopy images of MutuDCs treated with 33 μM GPN for 10 min. Cells were stained with DAPI (white) and for galectin-3 (magenta).

590 **(E)** MutuDCs were incubated with 0.5 mg/mL saporin for the indicated time in the presence or absence of 33 μM GPN. Following a 30 min puromycin chase, translation inhibition was monitored by flow cytometry. Data represent three independent experiments.

**(F)** CD11c+ enriched splenic DCs from C57BL/6J were incubated with saporin for 2 h, followed by a 30 min puromycin chase. Translation inhibition was monitored by flow cytometry. Data
595 represent mean and SEM for five independent experiments, ns, not significant; **, P<0.01 using a multiple unpaired t-test (two-stage step-up, Benjamini, Krieger and Yekutieli). For gating strategy see fig. S1C.

**(G)** $CD11c^{+}$ enriched splenic DCs from C57BL/6J or MRL/MpJ-$Fas^{lpr}$ were incubated with saporin for 2 h, followed by a 30 min puromycin chase. Translation inhibition was monitored by flow
600 cytometry. Data represent mean and SEM for two independent experiments each with two technical replicates, ns, not significant; *$P$<0.5; ** $P$<0.01; *** $P$<0.001; ****$P$<0.0001 using a multiple unpaired t-test (alpha = 0.5). For gating strategy see fig. S1C and fig. S1D.

Figure 2

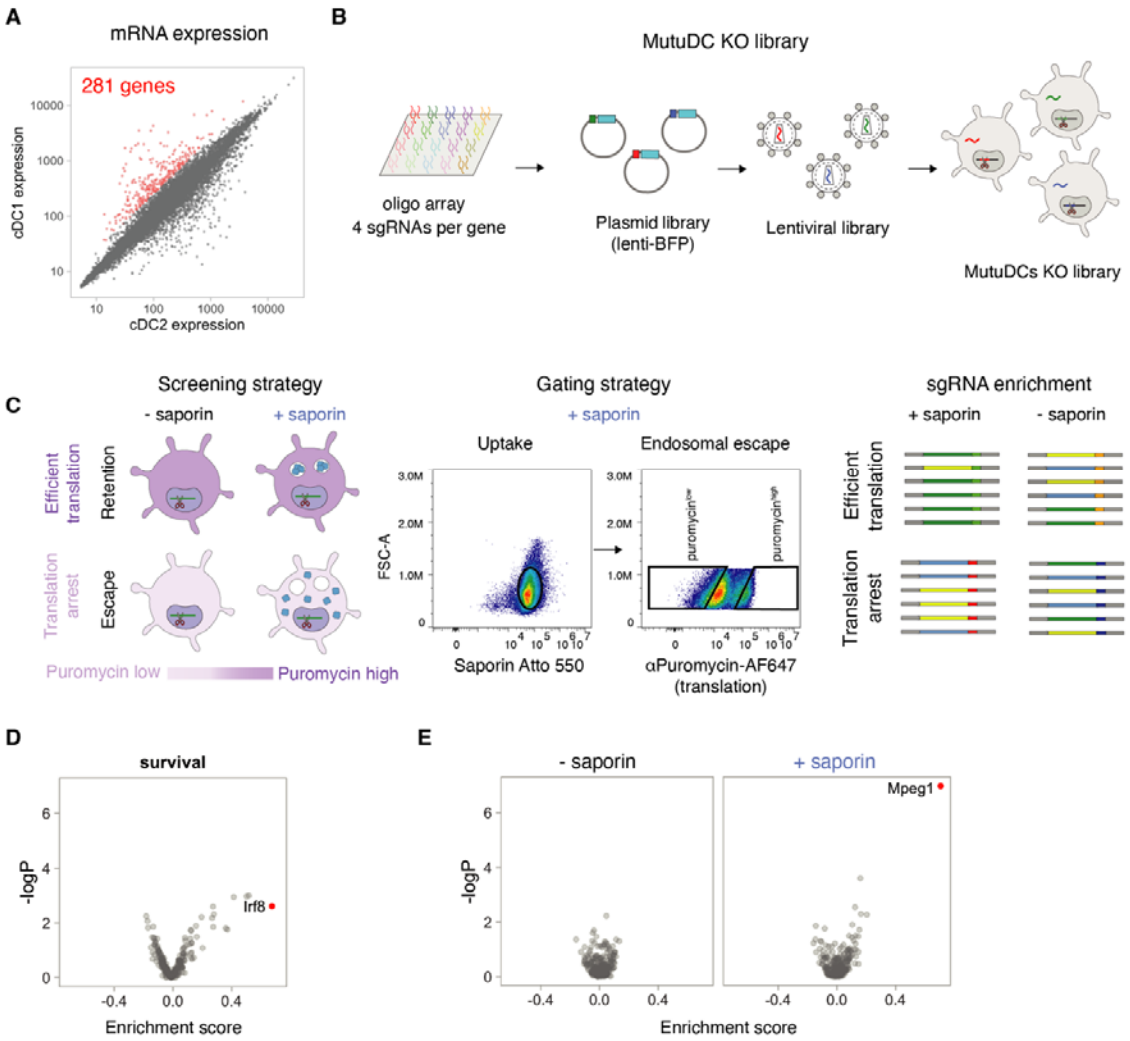


**Fig. 2 Genetic screen identifies Mpeg1 as a candidate regulator of endocytic escape in DCs.**

605 **(A)** cDC1 and cDC2 transcript comparison (data from the ImmGen consortium). 281 genes (coloured in red) met the log2(cDC1/cDC2) > 1.3 cut-off and were included in the CRIPSR/Cas9 library.

**(B)** The CRISPR/Cas9 library consisted of 4 sgRNAs per gene in a BFP-expressing lentiviral vector. Cas9-expressing MutuDCs were transduced with at an MOI of 0.3. Cells were sorted for

610 BFP expression and expanded.

**(C)** Schematic representation of the CRISPR/Cas9 screen. For the screen, the saporin-puromycin assay was performed with a 2 h pulse of 0.5 mg/mL saporin (1:11 ratio of saporin Atto550 to unlabelled). Cells were first gated on the basis of the Atto550 MFI, and cells with either high (saporin escape) or low (saporin retention) puromycin labelling were collected. Puromycin high

615 and low cells were also collected in the absence of saporin to identify guides that might have a

global effect on translation. Genomic DNA was then isolated and prepared for next generation sequencing of the sgRNAs.

**(D)** Volcano plot showing the sgRNAs enrichment analysis for the MutuDC library relative to the starting plasmid library. Each of the dots represents one targeted gene.

620 **(E)** Volcano plots showing the sgRNAs enrichment analysis for the indicated screens. Each of the dots represents one targeted gene. Data represent the combined mean enrichment scores and the non-adjusted p values from three independent experiments (Fisher's method).

Figure 3

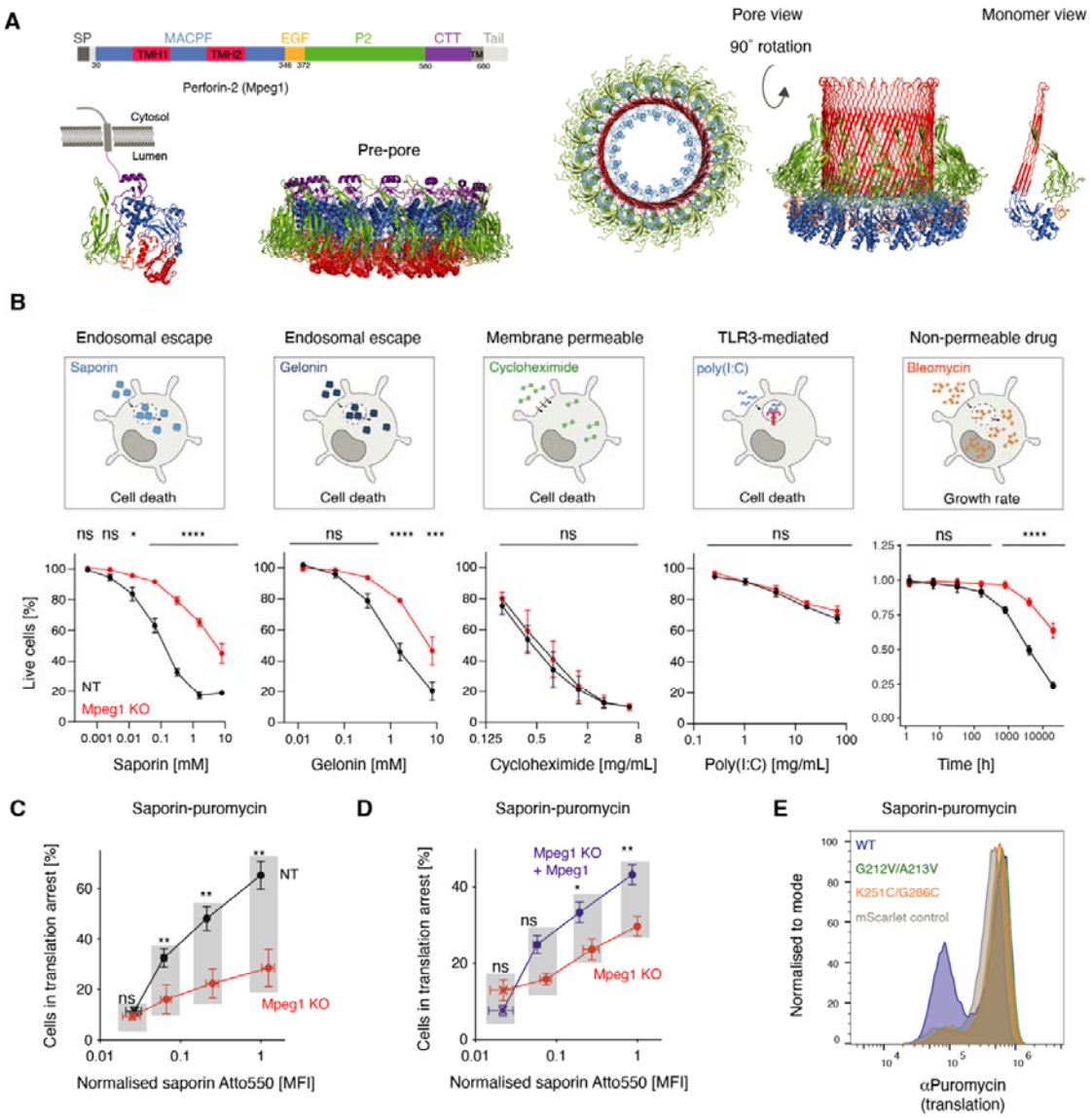


**Fig. 3 Perforin-2 facilitates endocytic escape of diverse cargo.**

**(A)** Schematic representation of the different perforin-2 domains alongside structures of single subunit and hexadecameric perforin-2 in pre-pore (PDB ID: 6U2K and PDB ID: 6SB3) and pore-forming conformations (PDB ID: 6SB5).

**(B)** *Mpeg1*$^{KO}$ and NT MutuDCs were treated for 24 h with either saporin, gelonin or cycloheximide or for 48 h with HMW-Poly(I:C). Cells were stained with a fixable live/dead stain, and viability was assessed by flow cytometry. For bleomycin, the cells were plated in the presence or absence of bleomycin and cultured in an Incucyte® for 48 h to monitor the growth rate. Data

represent mean and SEM of three independent experiments with four technical replicates each, ns, not significant; $^{*}P<0.5$; $^{**}P<0.01$; $^{***}P<0.001$; $^{****}P<0.0001$ using a multiple t-test (Bonferroni-Dunn).

635 **(C and D)** Quantification of translation arrest in (C) *Mpeg1*$^{KO}$ and NT MutuDCs or (D) *Mpeg1*$^{KO}$ and *Mpeg1*-complemented *Mpeg1*$^{KO}$ MutuDCs. Cells were pulsed with saporin (1:11, saporin-Atto 550:unlabelled) for 2 h, and translation was monitored by a 30 min puromycin chase. The X axis represents Atto 550 MFI, normalised to the (C) NT MutuDC or (D) *Mpeg1*$^{KO}$ MutuDCs Atto 550 MFI at the highest saporin concentration. Data represent mean and SEM of three independent
640 experiments, ns, not significant; $^{*}P<0.5$; $^{**}$ $P<0.01$; $^{***}$ $P<0.001$; $^{****}P<0.0001$ using a multiple unpaired t-test (two-stage step-up, Benjamini, Krieger and Yekutieli). Significance symbols in the plot refer to the differences in proportion of cells in translation arrest. Differences in saporin Atto 550 MFI were not significant.

**(E)** *Mpeg1*$^{KO}$ MutuDCs were reconstituted with the indicated *Mpeg1* mutants or with mScarlet
645 only and used in the saporin-puromycin assay with a 2 h pulse at 0.1 mg/ml saporin. Data are representative for three independent experiments.

Figure 4

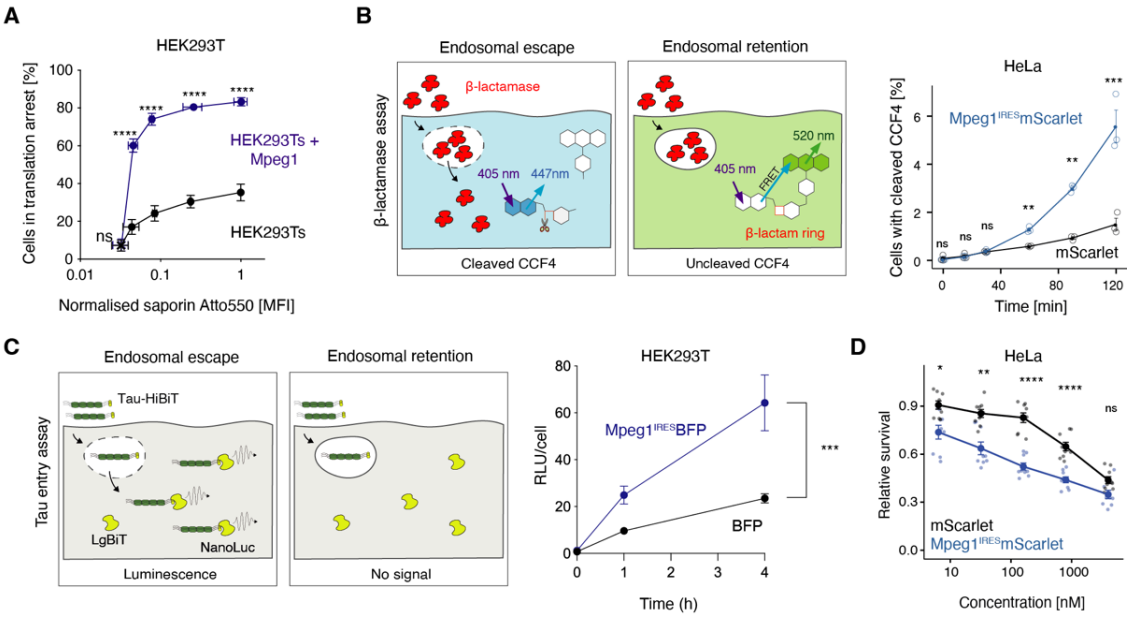


**Fig. 4 Perforin-2 is sufficient for endocytic escape of cargo in non-immune cells.**

**(A)** HEK293Ts and Mpeg1-complemented HEK293Ts were pulsed with saporin (1:11, saporin-Atto 550:unlabelled) for 2 h, and translation was monitored by a 30 min puromycin chase. The X axis represents Atto 550 MFI, normalised to the HEK293Ts Atto550 MFI at the highest saporin concentration. Data represent mean and SEM of three independent experiments, ns, not significant; * P<0.5; **P<0.01; ***P<0.001' ****P<0.0001 using a multiple t-test (Bonferroni-Dunn). Significance symbols on the plot refer to the differences in cells in translation arrest. Any differences in saporin Atto 550 MFI were not significant.

**(B)** Cytosolic escape of β-lactamase in cells loaded with the fluorescent β-lactamase substrate CCF4, results in cleavage of the substrate, loss of FRET and emission shift. HeLas expressing either *Mpeg1*$^{IRES}$-mScarlet or mScarlet-only were pulsed with β-lactamase for the indicated time. β-lactamase escape was monitored by measuring the shift in fluorescence emission by flow cytometry. Data represent mean and SEM of three independent experiments, ns, not significant, *$P$<0.5; **$P$<0.01; ***$P$<0.001; ****$P$<0.0001 using a multiple t-test (two-stage step-up, Benjamini, Krieger and Yekutieli) For gating strategy see fig. S3A.

**(C)** To monitor the escape of Tau oligomers, cells expressing NLS-eGFP-LargeBiT were pulsed with Tau-HiBit oligomers. The escape of Tau-HiBiT into the cytoplasm allows binding to the 18 kDA luciferase subunit, LgBiT. This results in reconstitution of catalytic activity and generation of luminescence. NLS-eGFP-LargeBiT HEK293Ts expressing either *Mpeg1*$^{IRES}$-BFP or BFP-only were pulsed with tau-HiBiT for the indicated time. Following substrate addition, luminesce and cell viability were assessed. Relative luminescent units (RLUs) were then normalised to viability per well. Data represent mean and SEM of three independent experiments each with six technical replicates, ***P<0.001 using a paired t-test.

**(D)** HEK293Ts were plated in the presence or absence of bleomycin and cultured in an Incucyte® for 48 h to monitor the growth rate. Data represent mean and SEM of three independent experiments with four wells per condition each, ns, not significant; $^{*}P<0.5$; $^{**}P<0.01$; $^{***}P<0.001$; $^{****}P<0.0001$ using a multiple t-test (Bonferroni-Dunn).

Figure 5

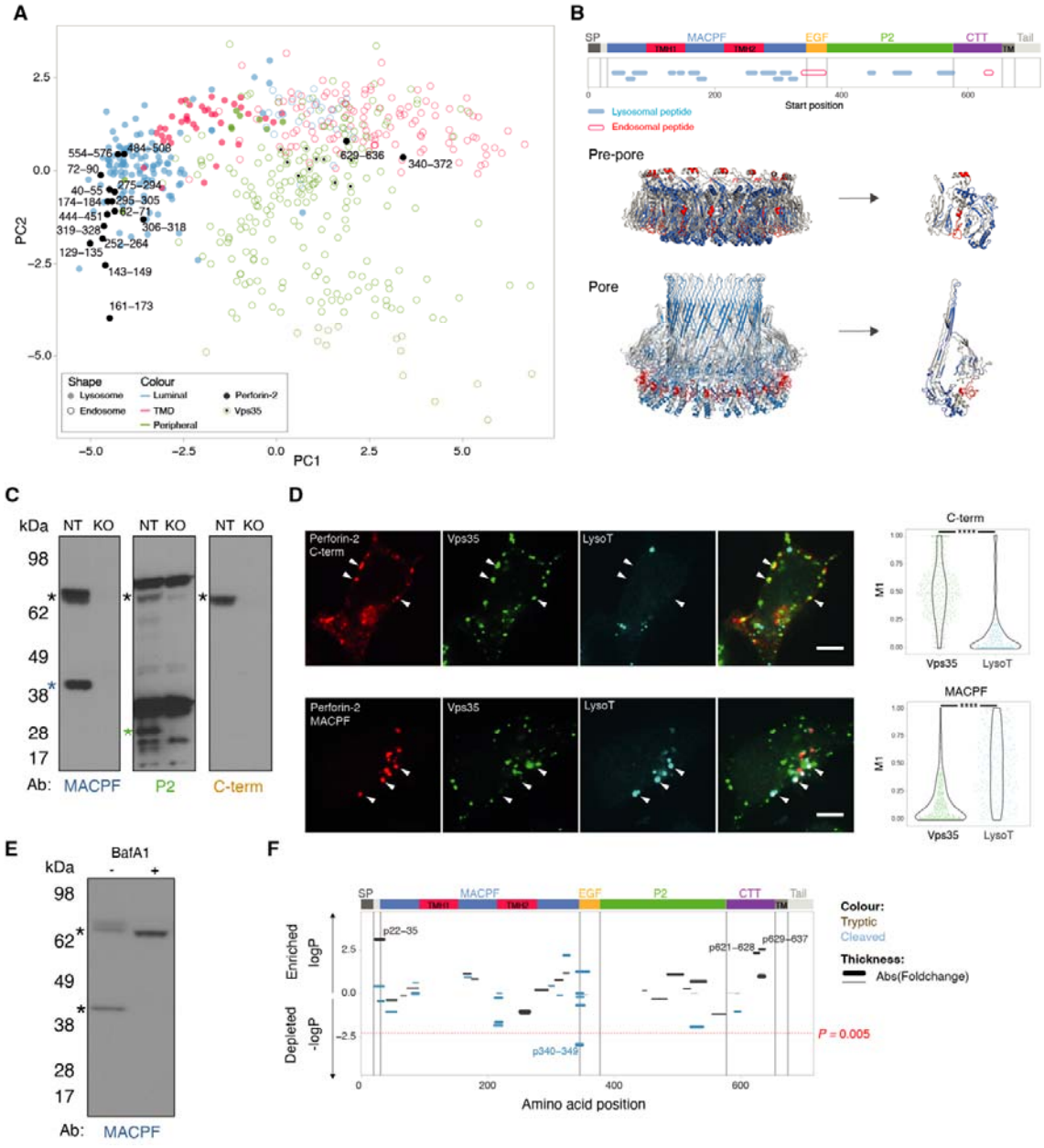


**Fig. 5 Perforin-2 undergoes proteolytic cleavage releasing its pore forming domain into the organellar lumen.**

**(A)** Principal component analysis of mass spectrometry-based organellar mapping of MutuDCs (*20*). Lysosomal proteins are represented by filled circles, while endosomal ones are indicated by empty ones. The different colours indicate localisation of the protein within the corresponding organelle. Perforin-2 peptides are displayed as filled black circles regardless of their localisation.

**(B)** Mapping of the different lysosomal and endosomal perforin-2 peptides detected by organellar mass spectrometry onto the different perforin-2 domains and structure.

**(C)** Perforin-2 levels in *Mpeg1*$^{KO}$ and NT MutuDCs were assessed by Western blot under non-
685 reducing conditions using several antibodies which recognise different perforin-2 epitopes. For ponceau staining see fig. S2E.

**(D)** Confocal microscopy images of MutuDCs stained for perforin-2 with either αC-terminal tail or αMACPF antibodies (red), Vps35 (green) and lysotracker (cyan). Data represent two independent experiments with at least 80 cells each. Statistical analysis was performed with a
690 Kolmogorov-Smirnov test.$^{***}P < 0.0001$.

**(E)** Perforin-2 levels in NT MutuDCs treated with 0.5 μM BafA1 for 3 h were assessed by Western blot under reducing conditions using the αMACPF antibody.

**(F)** BafA1 induced changes in the abundance of tryptic and cleaved perforin-2 peptides by full proteome mass spectrometry. Control and BafA1 (1 μM) treated cells were analysed by mass
695 spectrometry and peptide abundance was normalised per condition. Fold change in abundance of peptides in BafA1 vs control is shown and the amino acid position indicates the location of the peptides along the different perforin-2 domains. Two-sided student's t-test was used for statistical analysis. Multiple hypothesis correction was done by permutation based FDR with s0=0.1 using Perseus (table S2).

700

Figure 6

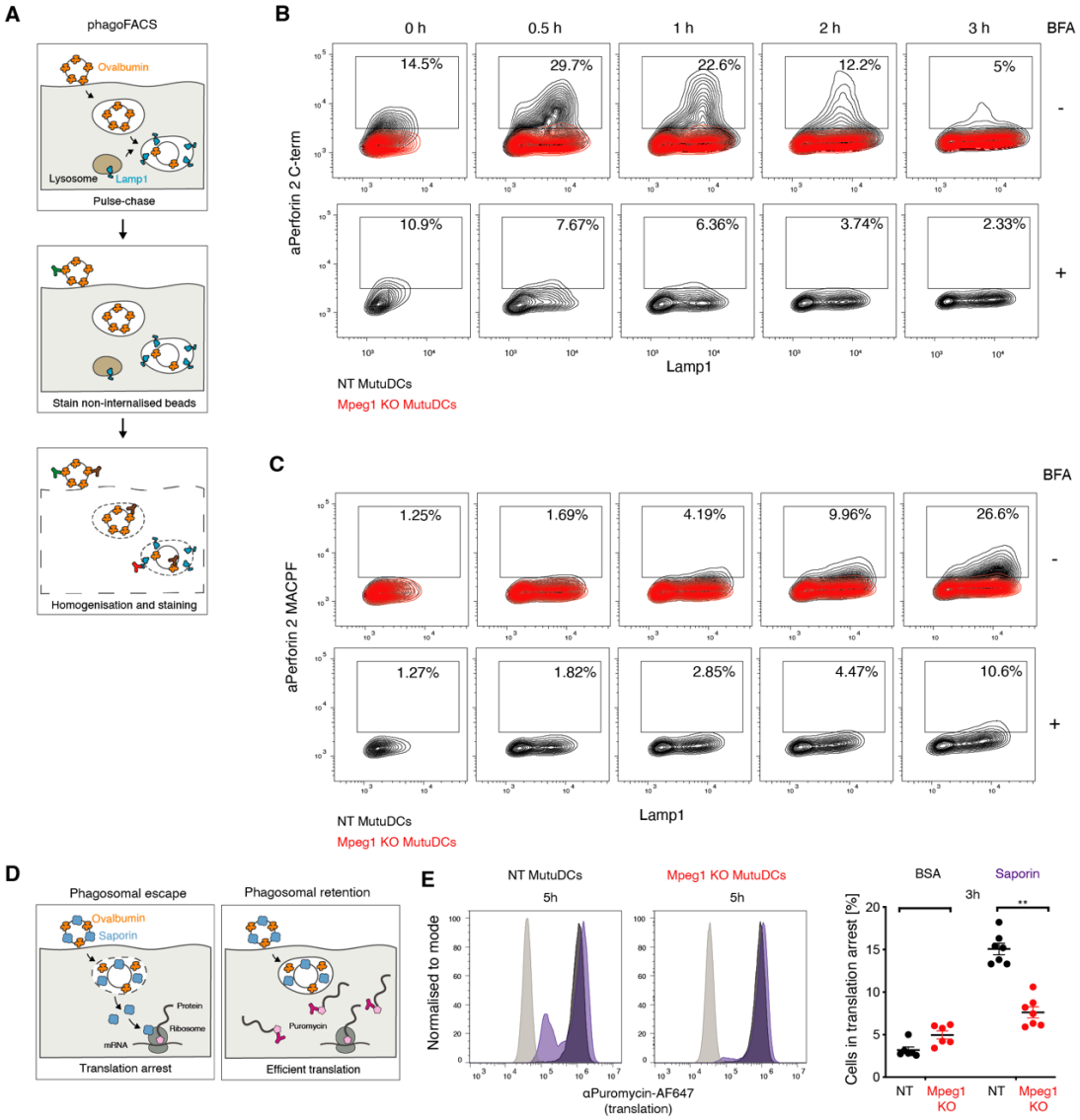


**Fig. 6 Perforin-2 undergoes pH-dependent proteolytic cleavage and mediates endocytic escape from antigen-containing phagosomes.**

**(A)** Schematic representation of the phagoFACS assay. Cells are pulsed with Ova-beads and allowed to internalise them. After an indicated chase period, non-internalised beads are marked with an αOvalbumin antibody. Following cell homogenisation, phagosomes are stained with antibodies against ovalbumin coupled to an alternative fluorophore and phagosomal markers.

**(B and C)** *Mpeg1*$^{KO}$ and NT MutuDCs were pulsed with Ova-beads and chased for the indicate time in the presence or absence of BFA. Isolated phagosomes were stained with antibodies against Lamp-1 and either the perforin-2 (B) C-terminus or (C) MACPF domain. Data are representative of three independent experiments. For gating strategy see fig. S6A.

**(D)** Schematic representation of the saporin-bead puromycin assay. Cells are pulsed with saporin-conjugated Ova-beads and allowed to internalise them for the indicated time. Translation is then monitored with a 30 min puromycin chase. Incorporated puromycin can then be detected with
715 an αPuromycin antibody and flow cytometry.

**(E)** *Mpeg1*$^{KO}$ and NT MutuDCs were pulsed for 3 or 5 h with saporin-conjugated Ova-beads and translation was monitored by a 30 min puromycin chase. Histograms are representative of two independent experiments each with two technical replicates. The quantification of translation inhibition represents three independent experiments each with at least two technical replicates,
720 ns, not significant; *P<0.5; **P<0.01; ***P<0.001; ****P<0.0001 using an unpaired t test. For gating strategy see fig. S6D.

Figure 7

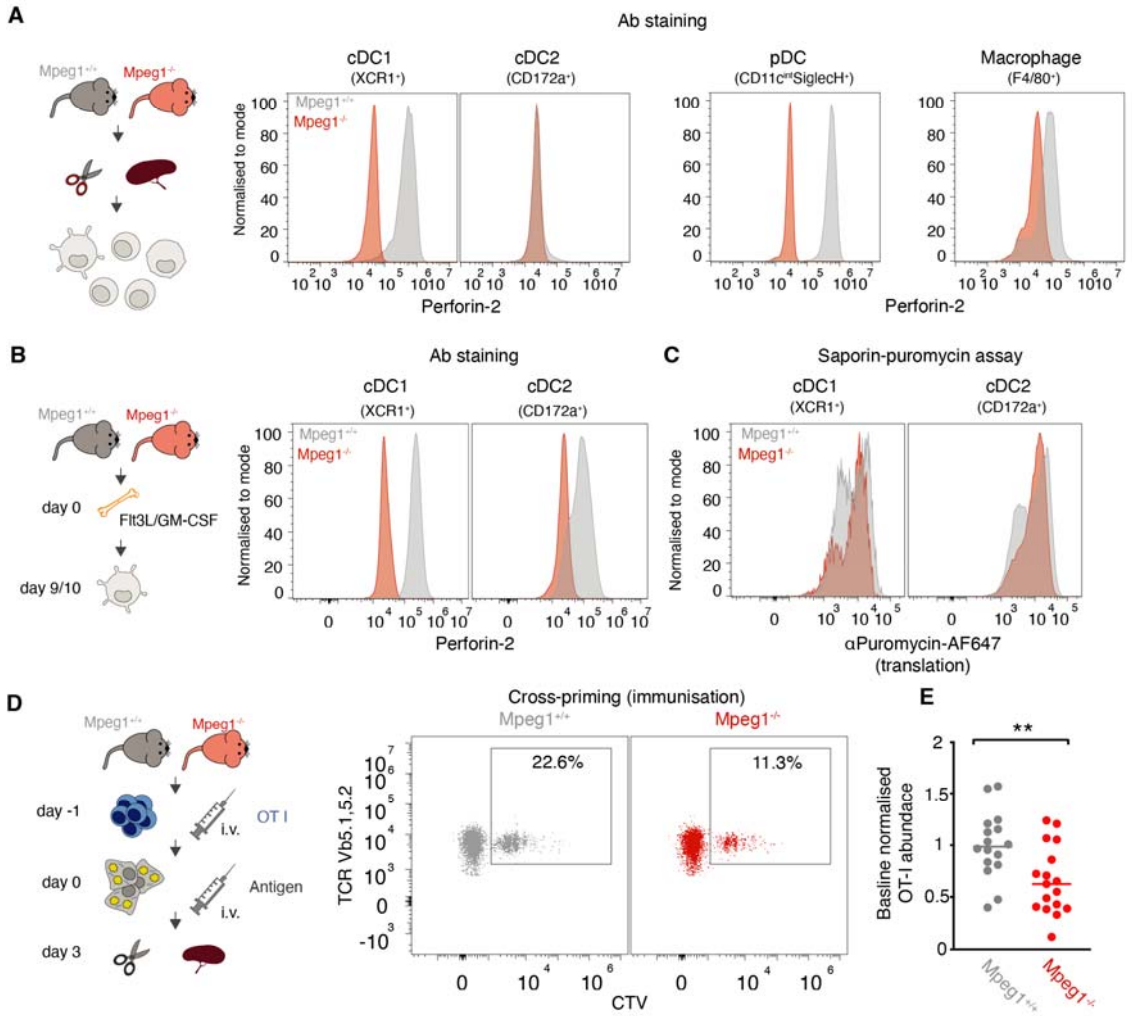


**Fig. 7 Antigen cross-presentation is impaired *in vivo* in the absence of perforin-2.**

**(A and B)** Perforin-2 expression was assessed by intracellular staining with an αPerforin-2 antibody and flow cytometry in (A) *Mpeg1*$^{+/+}$ and *Mpeg1*$^{-/-}$ splenocytes and (B) Flt3-L/GM-CSF bone marrow cultures. In (A), cDC1s are defined as Lineage (CD3, CD19, NK1.1)$^{-}$, F4/80$^{-}$, CD11C$^{+}$CX$_{3}$CR1$^{-}$, XCR1$^{+}$, cDC2s as Lineage (CD3, CD19, NK1.1)$^{-}$, F4/80$^{-}$, CD11C$^{+}$CX$_{3}$CR1$^{-}$, CD172a$^{+}$, pDCs as Lineage (CD3, CD19, NK1.1)$^{-}$, F4/80$^{-}$, CD11c$^{int}$SiglecH$^{+}$ and macrophages as Lineage (CD3, CD19, NK1.1)$^{-}$, F4/80$^{+}$. In (B), cDC1s are defined as F4/80$^{-}$, CD11c$^{+}$XCR1$^{+}$ and cDC2s as F4/80$^{-}$, CD11c$^{+}$CD172a$^{+}$. For gating strategies see fig. S7C and S8D.

**(C)** Flt3-L/GM-CSF bone marrow cultures from wild-type and *Mpeg1*$^{-/-}$ mice were pulsed with saporin for 2 h, and translation was monitored by a 30 min puromycin chase. Flt3-L/GM-CSF cDC1s and cDC2s are defined as in (B, see also fig. S7C). Histograms are representative for three independent experiments.

735 **(D)** Wild-type and *Mpeg1*$^{-/-}$ mice were intravenously (i.v.) injected with 0.5x10$^{6}$ CTV-labelled magnetically purified OT-I cells. One day later mice were i.v. injected with 1x10$^{6}$ UVC-irradiated (240mJ/cm$^{2}$) 3T3 cells, coated with 10 mg/mL ovalbumin and 0.5 mg/mL Poly(I:C). Three days later, OT-I proliferation was assessed by flow cytometry. OT-I are defined as Lineage (CD19, F4/80, CD11c)$^{-}$, CD3$^{+}$, CD4$^{-}$CD8$^{+}$, TCRvβ5.1, 5.2$^{+}$TCRvα2$^{+}$, CTV$^{+}$. For gating strategy see fig. S8F.

740 **(E)** Normalised OT-I counts three days after i.v. antigen injection. Each dot corresponds to an individual mouse, with three to five mice per group. For each experiment, OT-I counts per1x10$^{6}$ splenocytes were normalised to the average of wild-type controls. Data from five independent experiments, ns, not significant; $^{**}P<0.01$ using an unpaired t-test.